J. Phys. B: At. Mol. Opt. Phys. 25 (1992) 4553–4579. Printed in the UK

Near-threshold rotational excitation in electron–polar-molecule scattering

Helmar T Thümmel, Robert K Nesbet† and Sigrid D Peyerimhoff

Institut für Physikalische und Theoretische Chemie, Universität Bonn, Wegelerstraße 12, D-5300 Bonn, Federal Republic of Germany

Received 25 March 1992, in final form 8 July 1992

Abstract. Variational R-matrix calculations have been performed for electron scattering by the HF molecule. Calculations over a grid of internuclear distances are used to compute the vibronic R-matrix, using a new adiabatic phase matrix method described here. This body-frame vibronic R-matrix is converted to the rovibronic R-matrix by a modified frame transformation at the R-matrix boundary. The external rovibronic close-coupling equations are solved by analytic methods. This methodology makes it feasible to carry out full first-principles calculations including molecular rotation and vibration, although only vibrationally elastic results are reported in the present paper. The threshold behaviour of the body-frame results can be described in terms of dipole eigenfunctions. Validity and range of the analytic formula proposed by Clark are discussed quantitatively. Results in the laboratory frame show the influence of rotation on vibrationally elastic e–HF collisions. The computed cross sections at small energies, close to the rotational thresholds, show rather sharp peaks that are dominated by $j \rightarrow j \pm 1$ excitations. Analysis here shows that these peaks are multichannel threshold structures due to virtual states and that they are accompanied by threshold cusp structures. Scaling laws valid at rotational channel thresholds in the presence of the strong long-range dipole interaction are discussed. In the energy range of the rotational thresholds the differential cross section has a prominant forward peak. Good agreement is found with recent experimental results of Rädle *et al*. The present results are compared with approximations of various levels of sophistication.

1. Introduction

There has been great experimental (Rohr and Linder 1976, Knoth *et al* 1989, Rädle *et al* 1989), and theoretical interest (see, for example, the review of Morrison 1988) in recent years in the threshold behaviour of inelastic cross sections for electron scattering by polar molecules, especially the hydrogen halides. The long-range dipole interaction leads to large cross sections and to transfer of angular momentum of one unit. At low impact energies one has to include the rotational motion correctly in order to obtain reliable results on vibrational state-to-state transitions and the correct threshold behaviour. This is emphasized in the recent experimental work of Knoth *et al* (1989), who have investigated near-threshold electron impact excitation of HCl and HF. They found large contributions from rotational transitions with angular momentum transfer $\Delta j > 0$ (primarily $\Delta j = 1$ and 2) i.e. there is strong evidence

† Permanent address: IBM Almaden Research Center, San Jose, California 95120, USA.

0953-4075/92/214553+27$07.50 © 1992 IOP Publishing Ltd

for simultaneous vibrational and rotational excitation. Differential cross sections under the vibrational excitation peaks were found experimentally to show anisotropic angular dependence, which can be explained by interference of s,p,d waves in the exit channels.

The aim of the present work is, first, to study quantitatively the influence of a strong long-range dipole interaction as in e–HF on the threshold behaviour of scattering quantities such as K-matrix elements and eigenphase sums obtained solving the fixed-nuclei (FN) scattering equations in the molecule-fixed or body-frame of reference, and second, to consider molecular rotation in the space-fixed or laboratory frame of reference by using the frame-transformation method. Special emphasis is thus placed on rotational effects in the near-threshold energy region. We have chosen the HF molecule as a test case because of its large dipole moment. This provides a good example for checking the numerical accuracy of our methodology in the low-energy range. The calculations reported here are carried out over a grid of internuclear distances and vibronic scattering matrices are constructed, although the present paper will only discuss vibrationally elastic scattering. Vibrationally inelastic scattering will be considered in a subsequent paper.

2. Body-frame treatment

2.1. *Method of calculation*

There have been several publications which apply the R-matrix method to electron–molecule scattering. For a comprehensive review see Buckley *et al* (1984) and Burke and Noble (1986). In the R-matrix method, coordinate space is divided into a molecular core region, in which exchange and correlation effects are important, and an outer region in which only the long-range components of the interaction are considered. In the inner region a body-frame representation of the wavefunction is more appropriate. In the first stage of the R-matrix method electronic R-matrices are computed in the FN approximation. Wavefunctions for scattered electron and target electrons are calculated in the field of the nuclei, which are fixed in space. However, for near-threshold electron scattering or in the neighbourhood of narrow resonances, non-adiabatic effects of nuclear motion must also be included. Schneider *et al* (1979) have extended the R-matrix method to include non-adiabatic vibrational effects. In their work a generalized vibronic R-matrix is generated in the internal region of configuration space. This method has been used to compute cross sections for a number of diatomic molecules: $e^- + N_2$ scattering (Gillan *et al* 1987), $e^- + HF$ scattering (Morgan and Burke 1988) and $e^- + HCl$ scattering (Morgan *et al* 1990). In none of these applications have non-adiabatic rotational effects been included.

In the present work, FN electronic R-matrices are computed and then transformed to vibronic R-matrices by a modified adiabatic method, described later. FN R-matrices for HF scattering states of $^2\Sigma$ and $^2\Pi$ symmetry are computed in the body frame using variational R-matrix theory. This variational formalism places no condition on basis functions other than their linear independence (see e.g. Nesbet *et al* (1986) and references therein). The electronic orbital basis set used for HF is similar to that of Morgan and Burke (1988) and is summarized in table 1. It includes basis functions with angular momentum up to $l = 5$. The $^1\Sigma^+$ target wavefunction is an SCF wavefunction constructed by using the Slater-type orbital (STO) set given by McLean and Yoshimine (1967). This basis is augmented by continuum basis functions in the

form of regular spherical Bessel functions (RSB) and numerical asymptotic functions (NAFs) to ensure basis set convergence within the R-matrix radius. Following Morgan and Burke (1988) we have done the variational calculations at the static exchange plus short-range polarization (SEP) level for seven internuclear distances q in the range $1.3 \leqslant q \leqslant 2.3\ a_0$. In the SEP model charge polarization effects are taken into account by including single-particle virtual dipole excitations of the target valence electrons, described by correlation functions of two-particle–one-hole character. This is equivalent to the optical potential used by Schneider and Collins (1982).

Table 1. Orbital basis set. For further explanation see text.

		σ						π				
State	Basis	s	p	d	f	g	h	p	d	f	g	h
	STO^F	5	4	2	1			4	1	1		
	STO^H	3	3					1	1			
$^2\Sigma^+$	RSB	6	4	4	3	2	1					
	NAF	1	1	1	1	1	1					
$^2\Pi$	RSB							5	4	3	2	1
	NAF							1	1	1	1	1

Accurate variational treatment of electron scattering from molecules requires great computational effort; however consideration of the physics of low-energy electron scattering by small molecules indicates that such detailed calculations are necessary only for the lowest-order partial-wave states. This fact is exploited in the multichannel asymptotic distorted wave (ADW) approximation (Nesbet 1984), in which for high-order partial wave states the effective one-electron potential is modelled by retaining only the asymptotic multipole potentials outside an inner radius r_0 which is chosen so that the charge density lies primarily within r_0. Within our program package FN R-matrices are generated in the ADW approximation by solving the asymptotic close-coupling equations between r_0 and the R-matrix radius r_1. For the electron scattering from HF we choose $r_0 = 2.3\ a_0$ and $r_1 = 10\ a_0$. The ADW approximation is expected to be reliable for high partial-wave states and for scattering symmetries of large Λ, where Λ is the projection of the electronic angular momentum onto the body-fixed molecular axis. Test calculations on the $e^- + HF$ scattering system indicate that variational R-matrix elements having partial wave states with $l, l' > 5$ for $^2\Sigma$ and $^2\Pi$ symmetry and for symmetries with $\Lambda > 1$ can be approximated very well (differences of a few percent) by ADW. For our full scattering calculations we have included partial-wave states up to $l = 15$.

The asymptotic potential includes terms due to static dipole and quadrupole moments as well as isotropic and anisotropic polarizabilities. Where not explicitly stated, we have taken experimental values for the dipole moment as a function of internuclear distance from the measurements of Sileo and Cool (1976). For small distances up to $2.6\ a_0$ these values differ only slightly from theoretical results obtained performing large-scale *ab-initio* calculations. A detailed discussion is given by Werner and Rosmus (1980). For the ground vibrational state $\chi_{\nu=0}$ we obtain the following vibrationally averaged values: $D^{\nu\nu} = 0.715$ au (dipole moment), $Q^{\nu\nu} = 1.804$ au (quadrupole moment), $\alpha_0^{\nu\nu} = 5.593$ au (isotropic polarizability), $\alpha_2^{\nu\nu} = 0.962$ au (anisotropic polarizability). For the quadrupole moment we have used SCF values.

Table 2. Static polarizabilities of HF calculated from Botschwina (1991) as a function of the internuclear distance q.

q(Bohr)	$\alpha_{\parallel}(a_0^3)$	$\alpha_{\perp}(a_0^3)$
1.300	4.332	4.533
1.427	4.808	4.702
1.500	5.117	4.802
1.733	6.298	5.128
1.933	7.597	5.421
2.100	8.918	5.673
2.300	10.826	5.983

The polarizabilities as functions of internuclear distance are from CEPA calculations of Botschwina (1991), listed in table 2.

Vibrational motion is taken into account in the body frame. The electronic R-matrix for FN can, in principle, be computed to high accuracy by variational methods. This body-fixed R-matrix is computed for a range of electronic energies ϵ and a range of internuclear H–F distances q. Following the conceptual ideas of the energy-modified adiabatic approximation (EMA) of Nesbet (1979), the parameter ϵ becomes an operator $E - H_N$, equal to the net energy available to the electrons, when nuclear motion described by the Hamiltonian H_N is taken into account. The total energy E remains a pure number. In a basis of vibrational wavefunctions, the R-matrix takes the form of an extended matrix indexed by the vibrational quantum numbers. The matrix elements are integrals of the FN R-matrix, $R^{FN}(\epsilon_{op}; q)$, evaluated between vibrational eigenstates.

Although the R-matrix does not have branch-points as a function of the electronic energy parameter ϵ, it necessarily has a sequence of poles. Integration of such a function over the vibrational coordinate q, or interpolation in ϵ, is not expected to be accurate. In order to avoid this difficulty, the real symmetric matrix R^{FN} is replaced by an equivalent phase matrix Φ^{FN}, defined such that

$$R = \tan \Phi.$$

The matrix R is diagonalized and Φ is constructed from the eigenvectors and inverse tangents of the eigenvalues. Since these eigenphase elements are determined only modulo π, a phase map is created and multiples of π are introduced to ensure smooth behaviour in both parameters ϵ and q. Thus the vibronic phase matrix is

$$\Phi_{\nu l,\nu' l'}(E) \cong \langle \nu | \Phi^{FN}_{l,l'}(\epsilon_{\nu\nu'}; q) | \nu' \rangle \tag{1}$$

where

$$\epsilon_{\nu\nu'} = E - (E_\nu + E_{\nu'})/2. \tag{2}$$

The vibronic R-matrix is constructed from the tangents of the eigenvalues of this vibronic phase matrix. For a diagonal element, in vibrational state χ_ν, operator ϵ_{op} has a quantized numerical value $E - E_\nu$. The EMA associates intermediate numerical values with the operator ϵ in non-diagonal elements. Unlike the original application to the K-matrix, for which square-root threshold behaviour must be modelled, and only open channels, with positive ϵ, are considered, the R-matrix has

no comparable analytic branch-point structure. Hence a simpler approximation is appropriate, allowing values for ϵ of either algebraic sign. The present calculations use the arithmetic mean of the vibrational energies $E_\nu, E_{\nu'}$ for the non-diagonal elements.

Given the vibronic R-matrix or an R-matrix obtained in the FN approximation, calculations can proceed either in the body frame or in the laboratory frame, after a frame transformation to a molecular rotational basis, as described later. In either the body or laboratory frame, K-matrices are generated by fitting the relevant R-matrix to solutions of the asymptotic close-coupling equations, using a standard package of computer programs for the asymptotic region outside the R-matrix radius. The R-matrices are propagated outwards (Baluja *et al* 1982, Light and Walker 1976, Morgan 1984) to an external Gailitis radius r_g. For the solution in the external region we use the asymptotic code of Noble and Nesbet (1984).

2.2. *Body-frame results*

Direct calculations in the body frame imply an adiabatic approximation and summation over rotational states. For vibrationally elastic scattering, we have carried out calculations using two different representations of the vibronic R-matrix. The first method uses an FN R-matrix either with or without vibrational averaging, providing results that can be compared directly with prior analytic or model studies at this level of approximation. The second method, applied here primarily to rotationally non-adiabatic calculations, uses the vibrationally diagonal submatrix of the rovibronic R-matrix computed by the EMA phase matrix method.

In this section we discuss *ab-initio* results in the body frame obtained by solving the FN scattering equations. As discussed in an extensive literature, the FN approximation is valid in the limit that the classical collision time is much less than molecular vibrational or rotational periods (Norcross and Collins 1982). Neglect of the rotational Hamiltonian eliminates the coupling in Λ. In the case of electron scattering from polar molecules the validity of the FN approximation has generally been viewed as limited (see, e.g., reviews by Norcross and Collins (1982), Itikawa (1982) or Lane (1980)). An extreme example is the threshold behaviour of the FN eigenphase sum $\delta(E,\Lambda)$, which in the presence of a sufficiently strong long-range dipole interaction (D larger than a critical value D_{cr}) diverges at zero energy. In the FN approximation, a long-range dipole potential causes total integrated cross sections to diverge logarithmically, as discussed, for example, by Golden *et al* (1971). It will be shown in section 3 here that inclusion of molecular rotation eliminates this pathological behaviour.

Even if the dipole moment is less than critical ($D < D_{cr}$), the threshold behaviour of $\delta(E,\Lambda)$ is much more complicated than for non-polar molecules. As Clark (1984) has shown, in this case the eigenphase sum can be written as a sum of two terms

$$\delta(E,\Lambda) = \delta_D(E,\Lambda) + \sigma(D,\Lambda). \tag{3}$$

Whereas the second term σ depends only on the dipole moment and the value of Λ, the energy-dependent first term goes to zero with a power law which depends on other long-range potentials, such as the quadrupole and polarization potentials. In the case of a long-range r^{-2} potential the label l is no longer a good quantum number, even asymptotically. As a result, behaviour near threshold obeys a modified

threshold law determined by a new non-integer quantum label N that replaces l. For a pure dipole long-range potential (Clark 1984):

$$\delta_D(E,\Lambda)(\mathrm{mod}\,\pi) \sim E^{N+1/2} \qquad \text{as } E \to 0. \tag{4}$$

Clark has tabulated values for $\sigma(D,\Lambda)$, and one should, in principle, be able to verify the predicted values by *ab-initio* results. Previous *ab-initio* calculations for various polar systems (see review of Morrison, p 95) have not considered scattering energies close enough to threshold to test the behaviour implied by equation (3). Hence one major point in this section is to compare the present *ab-initio* results with the analytic theory of Clark.

2.3. *Threshold behaviour*

2.3.1. $^2\Sigma^+$ *scattering state.* The ground-state dipole moment of HF for the $^2\Sigma^+$ scattering state is greater than the critical value $\mu = 0.639$ au. The threshold scaling law predicts $\delta(E,\Lambda = 0)$ to be stepwise oscillatory (O'Malley 1965). In this section we use the SCF value of $D = 0.764$ au calculated at bond length of 1.7328 a_0. We follow the analysis given by Clark (1984) to investigate the threshold behaviour quantitatively in terms of dipole functions and compare the results of these calculations with those obtained using the standard asymptotic package based on the l representation of long-range interactions. The dipole-adapted basis is obtained by solving the Schrödinger equation in the asymptotic region, retaining only the dipole term in the interaction potential. The contribution from higher multipole terms dies off faster than r^{-2} and will be discussed later. The angular parts of the dipole functions $\Omega_N^{(\Lambda)}(\theta,\phi)$ are determined by the eigenvalue equation for the angular part of the asymptotic Schrödinger equation:

$$(l^2 - 2D\cos\theta)\Omega_N^{(\Lambda)} = N(N+1)\Omega_N^{(\Lambda)}. \tag{5}$$

$\Omega_N^{(\Lambda)}$ can be represented in spherical harmonics corresponding to the usual l-quantum numbers:

$$\Omega_N^{(\Lambda)}(\theta,\phi) = \sum_{l \geqslant |\Lambda|} A_{Nl}^{(\Lambda)} Y_{l\Lambda}(\theta,\phi). \tag{6}$$

We index the dipole functions by $n = 0, 1, 2, \ldots$ in the order of increasing values of $N(N+1)$, which also corresponds to the order of the dominant l character, rather than by the non-integral and, in general, complex value of N. For the $^2\Sigma^+$ state of the e^-+HF system only the first value of N is complex, leading to one attractive potential $N(N+1)/r^2$. This determines the low-energy behaviour of scattering quantities such as K-matrix elements and cross sections. The function corresponding to the lowest eigenvalue $N(N+1)$ possesses relatively large p and d components, indicating a strong mixing of partial waves due to the dipole interaction:

$$|n = 0\rangle = 1.00|s\rangle + 0.39|p\rangle + 0.05|d\rangle + \cdots.$$

Using dipole functions, the K-matrices can be generated as follows:

(i) transform the R-matrix to the dipole-adapted basis;

Table 3. Threshold behaviour of R- and K-matrix elements in the body-frame represented in the basis of dipole (N) functions (1 Ryd = 13.605 eV).

E(Ryd)	$R^N(0,0)$	$R^N(0,1)$	$R^N(1,1)$	$K^N(0,0)$	$K^N(0,1)$	$K^N(1,1)$	$K^N(0,0)^a$
0.000001	14.107	0.268	4.643	0.5469	0.0000	0.0000	0.5505
0.000005	14.110	0.268	4.643	0.3298	0.0000	0.0000	0.3320
0.00001	14.114	0.268	4.644	0.2605	0.0001	0.0000	0.2624
0.00005	14.145	0.270	4.646	0.1265	0.0002	0.0000	0.1281
0.0001	14.184	0.272	4.648	0.0754	0.0003	0.0000	0.0770
0.0005	14.507	0.285	4.668	−0.0383	0.0011	0.0000	−0.0367
0.001	14.933	0.303	4.693	−0.0881	0.0020	−0.0002	−0.0863
0.005	14.757	0.508	4.911	−0.2158	0.0085	−0.0021	−0.2119
0.008	14.584	0.806	5.096	−0.2595	0.0134	−0.0038	−0.2536
0.01	14.014	1.179	5.235	−0.2820	0.0167	−0.0047	−0.2746
0.05	−3.436	−0.911	11.353	−0.5238	0.0678	0.0148	−0.4614
0.1	0.409	0.550	−10.265	−0.7182	0.0669	0.0350	−0.5734

[a] These values are calculated using formula (7).

(ii) determine the values of the dipole functions and derivatives at the R-matrix radius;

(iii) compute the K-matrix in the dipole N representation; and

(iv) convert to the usual l representation using a non-unitary transformation similar to formula (12) of Clark (1984) in which he gives the relationship between $S_{l',l}$ and $S_{N',N}$. The relationship between the corresponding K-matrices can be easily derived since $S = (I + iK)(I - iK)^{-1}$.

In table 3, R- and K-matrix elements are given in the N-representation. For small energies the lowest N-state dominates, as can be seen from table 3. Only $K^N(0,0)$ survives as the energy goes to zero. Clark (1984) has derived an analytic formula for the threshold energy dependence of $K^N(0,0)$, which involves only three parameters, N, D and $R(0,0)$ at zero energy, that characterize the short-range interactions:

$$K^N(0,0) = \tanh(\tfrac{1}{2}\pi\mu)\tan(\mu \ln(\tfrac{1}{2}kr_1) - \phi + \xi) \tag{7}$$

where $\phi = \arg\Gamma(1 + i\mu)$, $\xi = \tan^{-1}(b/\mu)$. Here r_1 is the R-matrix radius, $k^2/2 = E$ is the total energy, μ is the imaginary part of N, $b = r_1/\mathrm{Re} - \frac{1}{2}$ and

$$\mathrm{Re} = \lim_{E \to 0} R^N(0,0) = 14.1.$$

Good agreement is found (see table 3) between the exact result for $K^N(0,0)$ and that from the analytic formula (7), which is a reasonable approximation for energies smaller than 0.01 Ryd. As an independent check of our asymptotic program package, K-matrices computed using the partial-wave representation in the asymptotic region can be compared with those obtained from $K^N(N,N')$. They agree well (table 4). The standard asymptotic package based on the l-representation gives accurate results down to energies very near the threshold.

Next we discuss the influence of the additional long-range potentials, which can easily be dealt with in the l representation. In figure 1(*a*), FN eigenphase sums, computed at the equilibrium internuclear distance with and without inclusion of the quadrupole moment ($\sim r^{-3}$) and static polarizabilities ($\sim r^{-4}$), are compared with the SEP results of Morgan and Burke (1988), who have included dipole and

Table 4. Threshold behaviour of K-matrix elements in the l representation.

E(Ryd)	$K^l(0,0)^a$	$K^l(0,1)^a$	$K^l(1,1)^a$	$K^l(0,0)^b$	$K^l(0,1)^b$	$K^l(1,1)^b$
0.000001	3.7590	0.2531	−0.1117	—	—	—
0.000005	2.2323	0.3140	−0.1141	—	—	—
0.00001	1.9257	0.3263	−0.1146	1.9221	0.3264	−0.1145
0.00005	1.4667	0.3448	−0.1153	1.4650	0.3449	−0.1153
0.0001	1.3255	0.3507	−0.1156	1.3242	0.3507	−0.1155
0.0005	1.0601	0.3625	−0.1162	1.0594	0.3625	−0.1161
0.001	0.9614	0.3677	−0.1166	0.9608	0.3676	−0.1166
0.005	0.7466	0.3843	−0.1200	0.7463	0.3842	−0.1199
0.008	0.6841	0.3925	−0.1225	0.6840	0.3924	−0.1224
0.01	0.6539	0.3975	−0.1239	0.6538	0.3975	−0.1239
0.05	0.3847	0.4664	−0.1005	0.3846	0.4664	−0.1005
0.1	0.2073	0.4637	−0.0734	0.2072	0.4637	−0.0734

[a] Obtained from $K^N(n,n')$.
[b] Calculated with the standard asymptotic package based on l representation.

quadrupole moments in the asymptotic potential. Following Morgan and Burke we omit partial-wave states higher than $l = 5$ in these calculations. The agreement between these two R-matrix calculations is excellent. Inclusion of static polarizabilities leads to an increase of the eigenphase sums on the order of a few percent.

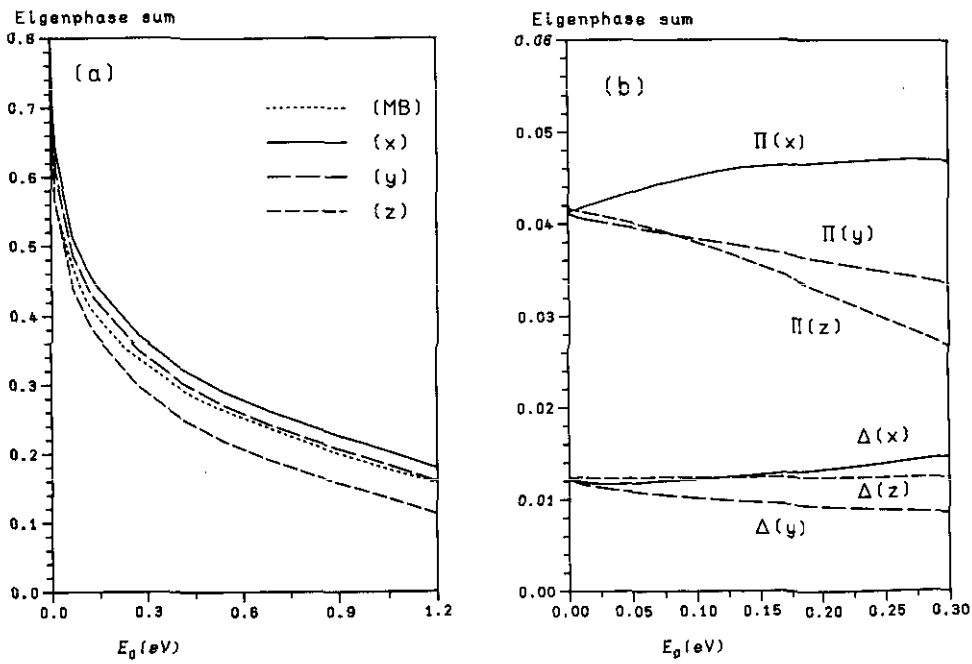

Figure 1. (*a*) Body-fixed eigenphase sums (rad) for the $^2\Sigma^+$ scattering state obtained from vibrational averaged R-matrices for different choices of the asymptotic potential: (x) inclusion of dipole-, quadrupole moment and polarizability; (y) neglect of polarizability; (z) pure dipole; MB theoretical results of Morgan and Burke (1988). (*b*) same as (*a*) for the $^2\Pi$ and $^2\Delta$ scattering states.

2.3.2. $^2\Pi$ *and* $^2\Delta$ *scattering states.* For these states the HF dipole moment is less than the critical value. In these cases all eigenvalues of equation (5) are greater than zero. Towards $E \to 0$ the eigenphase sums, according equation (3), go to constant values (figure 1(*b*)). Clark's formulas predict values of $0.0414(^2\Pi)$ and $0.0128(^2\Delta)$ for a dipole moment of 0.764 au. We find values of 0.0413 and 0.0123 for $^2\Sigma$ and $^2\Pi$, respectively, where l channels up to $l=15$ were included. The influence of long-range potentials other than the dipole term can be seen in figure 1(*b*). As was predicted by Clark (1977) the constant limit as $E \to 0$ is only affected by the dipole moment (first term of equation (3)). However, inclusion of polarizabilities as well as of the quadrupole term of the interaction potential has a large effect on eigenphase sums at higher energies.

3. Laboratory-frame treatment

3.1. Method of calculation

Frame-transformation theory (FT) was originally formulated by Chang and Fano (1972). The present implementation closely follows Chandra (1977). The novel aspect here is that the body-frame vibronic R-matrix, constructed from a variationally computed FN electronic R-matrix, as described earlier, is frame-transformed at the R-matrix boundary. Thus electronic exchange is treated exactly in the strong-interaction region of small electronic radii, non-adiabatic rovibrational coupling is treated exactly in the asymptotic region of large electronic radii, and the strongest electron–vibrational interaction is modelled in the inner region by the EMA phase matrix method. This formalism allows accurate calculations of electronic structure for FN to be combined with powerful analytic methods for integrating the rovibronic close-coupling equations in the asymptotic region, where the potential functions are long-range multipole potentials with simple analytic form. Our outer region computer program is designed to include vibrational motion (i.e. to start from a vibronic R-matrix) as well as to include several electronic target states. It includes eigenphase and resonance analysis, and calculation of the differential, total and momentum transfer cross sections.

Omitting the vibrational indices for the moment, the differential and integrated cross section for a rotational transition $j \to j'$ (Arthurs and Dalgarno 1960, Chandra 1977) can be written as

$$\frac{\mathrm{d}\sigma_{j\to j'}}{\mathrm{d}\Omega} = \frac{k_j^{-2}}{4(2j+1)} \sum_L [A_L^{jj'}] \times P_L(\cos\theta) \tag{8}$$

$$\sigma_{j\to j'} = \frac{\pi k_j^{-2}}{2(2j+1)} A_0^{jj'}.$$

The coefficients $A_L^{j,j'}$ depend explicitly only on the transition matrix $T^{J\eta}(lj, l'j')$ and on algebraic factors. The precise definition is not of interest here, but it involves (in principle) infinite sums over angular momenta l', l as well as a summation over total angular momenta J and parity quantum number η. The coupled equations for electron scattering by a heteronuclear diatomic molecule such as HF in its $^1\Sigma^+$ electronic ground state can be decomposed into two different sets, according to

the parity quantum number $\eta = (-1)^{J+j+l}$, for the same value of J. Rotational transitions involving higher rotational states generally require the solution of the laboratory-frame scattering equations for large values of J. It is well known that for electron scattering from a polar molecule the dipole interaction leads to extremely slow convergence in J. At low-impact energies (of the order of a few eV) the slow convergence not only affects transitions with $\Delta j = 1$ directly coupled by the dipole interaction but also $\Delta j = 0, 2$ transitions due to higher-order effects. As will be discussed in the next section, transition matrix elements for large J are in good agreement with those calculated in the first Born approximation (FBA) or the unitarized first Born approximation (UFBA). UFBA (Seaton 1961, 1966; Levine 1969a) not only satisfies the requirement of unitarity of the transition matrix but also accounts to some extent for second-order interactions ($\Delta j, \Delta l \neq 1$) not allowed in the Born dipole approximation. In the present treatment we replace the exact transition matrix elements for J larger than a certain value $J_{\max}$ for transitions with $\Delta j = 0, 1, 2$ by the corresponding elements in the Born approximation, yielding the following formulae for the differential and integrated cross section (Chandra 1977):

$$\frac{d\sigma_{j\to j'}}{d\Omega} = \frac{d\sigma^{B}_{j\to j'}}{d\Omega} + \frac{k_j^{-2}}{4(2j+1)} \sum_L [A_L^{jj'} - {}^{B}A_L^{jj'}] \times P_L(\cos\theta)$$

$$\sigma_{j\to j'} = \sigma^{B}_{j\to j'} + \frac{\pi k_j^{-2}}{2(2j+1)} [A_0^{jj'} - {}^{B}A_0^{j,j'}]. \tag{9}$$

The first term of equation (9) is the FBA for the differential cross section, which can be evaluated in closed form for all terms of the asymptotic potential (see, for example, Chandra 1977). As in the ADW approximation (section 2.1), an inner cutoff radius $r_0 = 2.3\ a_0$ is used for all FBA calculations here. The ${}^{B}A_L^{j,j'}$ coefficients are computed from FBA transition matrices. Our implementation of the first Born approximation uses a new algorithm based on conversion of indefinite integrals to continued fractions (Nesbet 1992). The potential consists of the dipole and quadrupole terms as well as the polarizabilities.

The whole procedure of employing the frame transformation can be divided into the following steps:

(i) Solve the FN equations in the inner region using the variational R-matrix method and compute the body-frame $R^{\Lambda}_{ll'}(\epsilon, q)$ matrices.

(ii) Study the convergence in l, l' of the variational results and use the ADW approximation, which becomes more and more valid for higher partial-wave states and for increasing Λ (see section 2.1).

(iii) Generate the vibronic R-matrix in the body frame using an adiabatic method such as the EMA phase matrix method, or, alternatively, include non-adiabatic vibrational effects using a method such as that proposed by Schneider *et al* (1979).

(iv) Transform $R^{\Lambda}_{\nu l,\nu' l'}$ obtained at the R-matrix radius r_1 to the laboratory-frame R-matrices $R^{J\eta}_{\nu jl,\nu' j' l'}$. Here J is the total angular momentum, and j, j' are the target rotational quantum numbers.

(v) Solve the coupled equations in the outer region for each η and J up to a certain value $J_{\max}$ to obtain $K^{J\eta}_{\nu jl,\nu' j' l'}$ and the transition matrix $T^{J\eta}_{\nu jl,\nu' j' l'}[T = K(I - iK)^{-1}]$. Convergence of the laboratory-frame calculations, i.e. the number of coupled (jl) basis states for each J and η, can be studied using eigenphase analysis of the K-matrices.

(vi) Calculate partial cross sections $\sigma^J_{vj\to v'j'}$. Check convergence of $\sigma^J_{vj\to v'j'}$ in J and η. Check the validity of FBA and UFBA for $J > J_{max}$. Since J and η are conserved quantum numbers in the laboratory-frame, threshold scaling laws and resonances can be investigated at this stage from an analysis of the matrix elements $K^{J,\eta}$ and the corresponding eigenphase sums.

(vii) Use the Born closure procedure according to equations (9) for the final calculation of the cross sections.

Our laboratory-frame asymptotic program package is designed to solve up to 100 coupled equations. The same integration methods as in the body frame are used for solving the rovibrational close-coupling equations (section 2.1). Usually for each J the expansion includes all basis functions with $j \leqslant j_{max}$ and $|J - j| \leqslant l \leqslant |J + j|$. The limit j_{max} is increased until convergence is reached.

For a direct comparison with experiment the initial population of rotational states should be determined according to the Boltzmann distribution law. For their experiments, Rädle *et al* (1989) give an average temperature of 400 K. At this temperature, the rotational state distribution for HF has a significant population (larger than 1%) up to $j = 7$. However, since the maximum contribution to the cross section comes from the coupling of the lowest partial waves $l = 0$, 1 and 2 in the present calculation, we truncate the basis so that it includes only those functions with $l, j \leqslant 7$ for $J \leqslant 5$ and with $l, j \leqslant J + 2$ for $J > 5$. The rotational constant of HF was assigned the value $B = 2.59$ meV (Sileo and Cool 1976). A Gailitis radius as large as $r_g = 2700\ a_0$ was used for energies near rotational thresholds.

3.2. Laboratory-frame results

Since scattering quantities such as K-matrix elements and partial cross sections depend critically on the radius r_F at which the frame transformation is performed (Chandra 1977, Vo Ky Lan *et al* 1983) we first checked our methodology by investigating the effect of varying r_F (section 3.2.1). In section 3.2.2 the convergence in J in the outer region as well as the validity of the Born approximation is studied. The scattering results at impact energies on the order of, or less than the rotational constant B are considered in section 3.2.2. In section 3.2.3 we give the results at larger impact energies in the range from 0.6 to 6 eV.

3.2.1. Dependence on the frame-transformation radius. We have performed test calculations varying the frame-transformation radius r_F in order to examine its effect on the largest K-matrix elements. Clark (1979) estimates a lower limit E_{min} for the collision energy for which the frame transformation is valid. In our numerical tests we vary r_F in the range from 7 to 20 a_0. For r_F less than the R-matrix radius r_1 of 10 a_0 we simply propagate the body-frame R-matrices backwards using the asymptotic potentials determined by the dipole moment, quadrupole moment and polarizabilities. For $J > 0$ the largest K-matrix elements relevant to the threshold peak at $E_{j=J}$ are $K^J_{ss}(K^J_{0J,0J})$, $K^J_{ps}(K^J_{1J-1,0J})$, and $K^J_{pp}(K^J_{1J-1,1J-1})$. K^J_{ss} corresponds to elastic scattering $j = J \to J$ in the new channels opening at threshold, K^J_{ps} to the rotational excitation $j = J - 1 \to J$ (outgoing s-wave) and K^J_{pp} is the largest contributor corresponding to background scattering in the old channels $j = J - 1 \to J - 1$. As an example we give results for the scattering state of total angular momentum $J = 2$ and $\eta = +1$. The energy behaviour of these matrix elements K_{pp}, K_{ps} and K_s as a function of E_0 is shown for different values of r_F in figures 2(*a*)–(*c*), respectively,

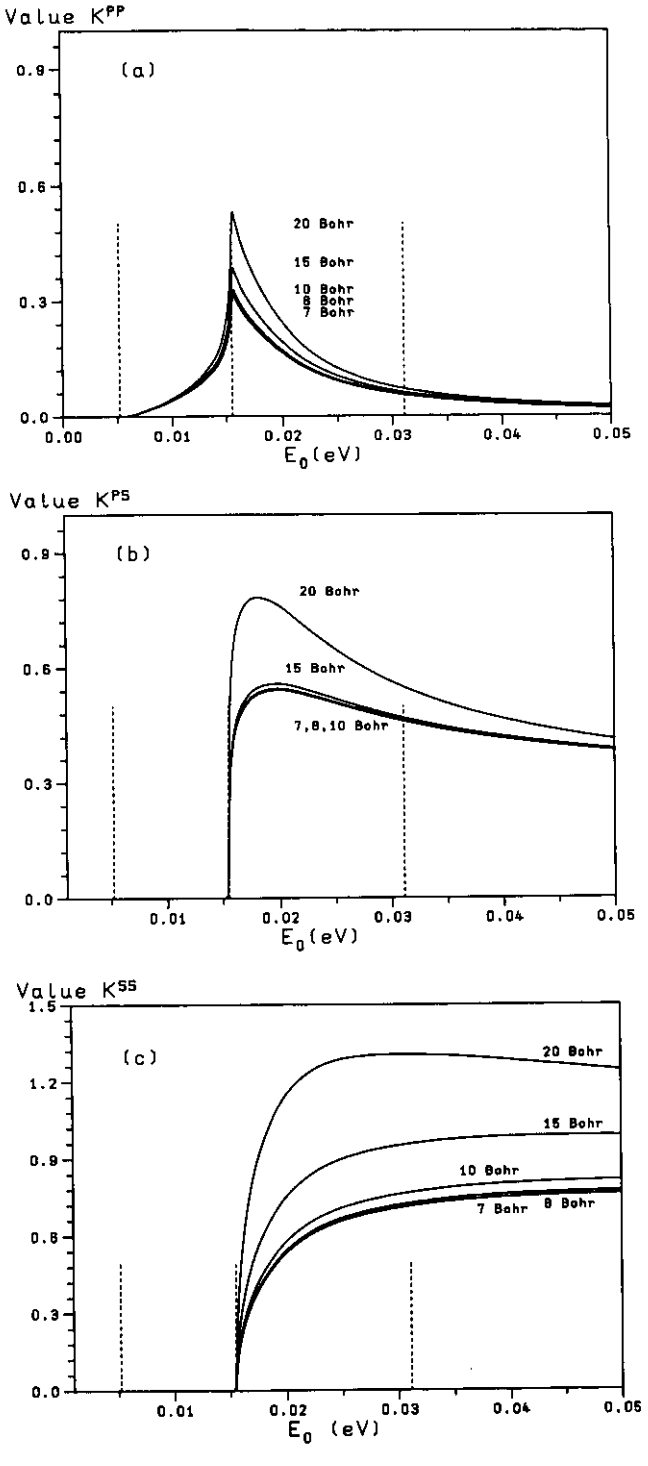

Figure 2. (*a*) Dependence of the K-matrix element $K^{J=2}_{1J-1,1J-1}$, (K_{pp}) on the frame transformation radius. The successive curves starting from the top correspond to $r_F = 20, 15, 10, 8$ and $7a_0$,respectively. The vertical broken lines indicate the thresholds $E_{j=0,1,2}$. (*b*) Same as (*a*) for $K^{J=2}_{0J,1J-1}$, (K_{sp}). (*c*) Same as (*a*) for $K^{J=2}_{0J,0J}$, (K_{ss}).

where E_0 is the energy of the electron incident on the ground rovibronic state of HF. The incident electron energy for a molecule in rotational state j is given by $E_{inc} = E_0 - Bj(j+1)$ where B is the rotational constant. As expected (Vo Ky Lan *et al* 1983), the strongest dependence on r_F is found for the diagonal K_{ss}-matrix element, corresponding to rotational elastic scattering $j = 2 \rightarrow 2$ and for decreasing energies i.e. near thresholds. Our tests indicate that, in the case of the HF molecule, converged results are obtained for $r_F = 7\ a_0$, and the results for $r_F = 10$ bohr even at energies close to thresholds are still satisfactory. For larger r_F the results diverge rapidly.

3.2.2. Convergence in the outer region. Within our methodology the solution of the laboratory-frame scattering equations in the outer region for each J and parity value η is the most time-consuming part. Furthermore the consideration of higher values of J will also mean that one has to calculate the R-matrix elements $R^{\Lambda}_{vl,v'l'}$ for higher values of Λ, since $|\Lambda| \leqslant min(l, j)$. So it is necessary to consider approximations for high J values and to determine their ranges of validity. In electron–molecule scattering rotational transitions with small angular momentum transfer usually dominate (Shimamura 1984). The calculated partial cross sections $\sigma^J_{0\rightarrow j'}$ with $j' = 0, 1, 2$ are compared with those calculated in the FBA and the UFBA for different incident energies of 0.047, 0.63 and 6 eV in table 5. One first notices from table 5 the very slow rate of convergence for $\Delta j = 1$ transitions for which, depending on the energy range, as many as 100 values of J would be required. The energy dependence $\sigma^J_{j=0\rightarrow 1}$ in the near threshold region is shown in figure 3. At very low impact energies, below the opening of the rotational channel $j = 2$, partial cross sections with $J \neq 1$ are only a few percent of the $\sigma^{J=1}_{0\rightarrow 1}$ partial cross section.

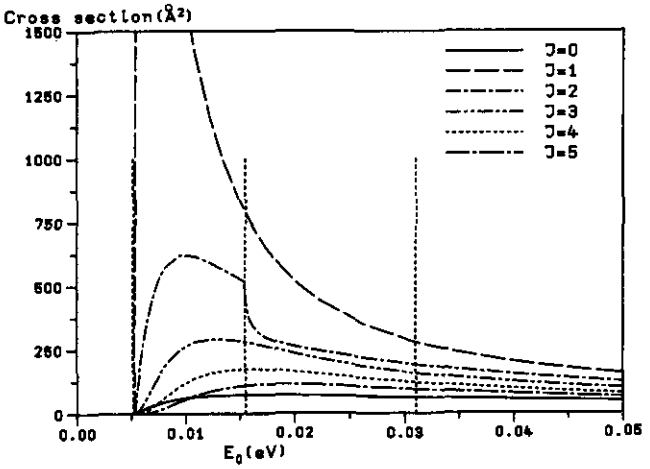

Figure 3. Partial cross sections $\sigma^J_{j=0\rightarrow 1}$ as a function of incident energy. The rotational thresholds $E_{j=1,2,3}$ are indicated by broken vertical lines.

As can be judged from the Born dipole approximation, the individual contributions $\sigma^J_{j\rightarrow j\pm 1}$ to the total cross section $\sigma_{j\rightarrow j\pm 1}$, which are due to the dipole interaction, generally become distributed over individual J with increasing energy. Especially at low impact energies, the scattering is mainly determined by the dipole interaction.

Table 5. Individual contributions $\sigma^J_{0\to j}$, for positive η and incident energies of 0.047, 0.63 and 6 eV: (*a*) present *ab-initio* results; (*b*) results of FBA; (*c*) UFBA.

		$E = 0.047$ eV			$E = 0.63$ eV			$E = 6$ eV		
J		0→0	0→1	0→2	0→0	0→1	0→2	0→0	0→1	0→2
0	*a*	34.253	47.815	0.6225	13.367	8.827	0.4737	0.9725	0.9977	0.3351
	b	15.557	114.413	0.0193	6.3583	10.428	0.0529	0.2295	0.2449	0.0069
	c	21.951	89.952	0.8147	5.2446	7.148	0.2803	0.8942	0.1955	0.0076
1	*a*	15.423	167.204	18.321	1.8258	14.421	2.3645	5.5699	1.7987	0.3317
	b	0.0430	280.801	0.4903	0.3689	17.471	0.6647	0.6817	0.8043	0.2843
	c	19.521	214.543	20.044	1.0371	12.769	0.9346	0.4933	0.6711	0.2193
2	*a*	4.3766	131.092	12.573	0.3168	9.674	0.6852	0.2004	1.2749	0.4290
	b	0.0016	159.057	0.2107	0.0225	10.824	0.1587	0.1589	1.0059	0.1018
	c	3.8990	125.387	11.611	0.2809	9.288	0.4835	0.1541	0.8837	0.0922
3	*a*	1.7111	104.276	2.9580	0.1087	7.2284	0.1513	0.0237	0.8334	0.0368
	b	0.0003	111.327	0.0618	0.0036	7.5975	0.0467	0.0330	0.7866	0.0458
	c	1.5854	101.923	2.6517	0.1053	7.1172	0.1602	0.0394	0.7326	0.0482
4	*a*	0.8091	83.097	1.2695	0.0498	5.6673	0.0638	0.0135	0.6496	0.0200
	b	0.0000	84.818	0.0269	0.0094	5.8685	0.0845	0.0084	0.6113	0.0205
	c	0.7467	80.830	1.1994	0.0495	5.6568	0.0722	0.0134	0.5882	0.0235
5	*a*	0.4390	66.547	0.5672	0.0268	4.6455	0.0339	0.0033	0.5198	0.0074
	b	0.0000	67.687	0.0139	0.0003	4.7886	0.0103	0.0032	0.4982	0.0106
	c	0.3962	65.780	0.5569	0.0272	4.6762	0.0381	0.0058	0.4866	0.0126
8	*a*	—	—	—	0.0070	2.9745	0.0083	0.0011	0.3181	0.0030
	b	—	—	—	0.0000	3.0967	0.0027	0.0003	0.3209	0.0027
	c	—	—	—	0.0074	3.0673	0.0099	0.0011	0.3180	0.0033

Here second-order effects of the dipole interaction imply for $\Delta j = 0$ and 2 rotational transitions a similar rate of convergence in J to that found for $\Delta j = 1$ transitions. The UFBA accounts to some extent for second-order effects. As can be judged from a comparison between the FBA and UFBA, the slow convergence for $\Delta j = 0, 2$ at low impact energies is due to the long-range dipole term. Here the quadrupole term and static polarizabilities are responsible only for a few percent of the contribution to the $\sigma^J_{j=0\to 0,2}$ cross sections. For large J the UFBA seems to be an excellent approximation in the low-energy range for transition matrix elements corresponding to small angular momentum transfer $\Delta j = 0, 1, 2$. At larger impact energies contributions due to short-range effects, polarizabilities, and the quadrupole term of the interaction potential gain relative importance and also affect the partial cross sections $\sigma^J_{j\to j\pm 1}$, in particular for the lowest J. Hence for absolute values there is a faster rate of convergence in J for all rotational transitions with $\Delta j = 0, 1, 2$ at higher energies. In our final calculations of cross sections, using Born closure according to equations (9), we solved the rovibronic close-coupling calculations up to $J_{max} = 9$ including only one vibrational state in the near threshold region (results of section 3.2.3) and up to $J_{max} = 6$ for higher energies (results of section 3.3), including three vibrational levels in the vibronic R-matrix to achieve convergence for the vibrationally elastic cross section.

3.2.3. Results for near-threshold rotational excitation. As discussed in section 2.3, in the body frame (BF) there is a strong coupling between the lowest partial waves due to the long-range dipole potential. At small impact energies, this leads to logarithmic behaviour of the BF eigenphase sums obtained in FN approximation for the $^2\Sigma^+$ scattering state (formula (7)), and for arbitrary Λ to divergent terms in the FN cross sections as the energy goes to zero. The purpose of this section is to investigate quantitatively the low-energy behaviour of cross sections, eigenphase sums and leading K-matrix elements in the laboratory frame, as modified by molecular rotation.

The multichannel theory of threshold effects has been summarized by Brandsden (1970) and Nesbet (1975, 1980). As was shown by Fabrikant (1983), the strong dipole moment of molecules such as LiF or HF leads to very narrow resonance-like structures near threshold. Such structures probably cannot be observed directly in the excitation cross sections, but should be observable in photo-detachment cross sections whenever the corresponding anion exists. Photodetachment thresholds resulting from electron–dipole interaction were discussed by Engelking and Herrick (1984). The FN approximation in the body frame is physically equivalent to the rigid rotor (RR) approximation in the laboratory frame: in both representations the vibrational motion is neglected and the internuclear separation is fixed at the equilibrium value of 1.7328 a_0. In analogy to section 2.3 we therefore have performed calculations in the RR approximation in order to investigate the influence of molecular rotation on the FN results. In figure 4 eigenphase sums for different choices of J and η are shown as a function of the energy E_0. As in section 2.3, we chose the value for the dipole moment of $D = 0.764$ au. For $\eta = +1$ the curves show a typical pattern similar to results obtained by Fabrikant (1983) using effective-range theory: for each J curve there is the steep (nearly vertical) rise at the threshold $E_{j=J}$. At higher energies the eigenphase sums get closer and closer to the values obtained in the adiabatic nuclei rotational (ANR) approximation, as discussed by Fabrikant. Technically the ANR values are those which can be obtained by doing the frame transformation at the level of asymptotic body-frame K-matrices. Physically this assumes that the scattering function is insensitive to the nuclear dynamics and also that the initial and final target states are degenerate. The ANR model is expected to be successful at higher energies but will fail near thresholds (for a discussion see Morrison (1988, p 82)). The eigenphase sums for negative η, also shown in figure 4, are much smaller, since s-partial waves are missing in the rotational basis set. A test was performed varying the dipole moment D. The corresponding eigenphase sums for calculations in the RR approximation for $J = 1$ are shown in figure 5. Nothing special happens in going from a 'critical' dipole moment of 0.764 to a 'non-critical' value of 0.63 au. Reducing D to half of its value leads to an appreciable reduction in the eigenphase sum by about one half in the near threshold region, indicating the dominant influence of the dipole moment in e^-–HF scattering. With the exception of the results in the RR approximation discussed earlier vibration is included using the EMA phase matrix method.

Now the questions ariseas to what the threshold laws for cross sections and K-matrix elements near the rotational thresholds are and, furthermore, whether the implied threshold structures are associated with resonances, bound states or virtual states.

As a first point we discuss the influence of the dipole interaction on the electronic s-wave and consider the low-energy behaviour of K^J_{ss} corresponding to the rotational elastic scattering $j = J \rightarrow J$ above the threshold $E_{j=J}$. From the theory of the

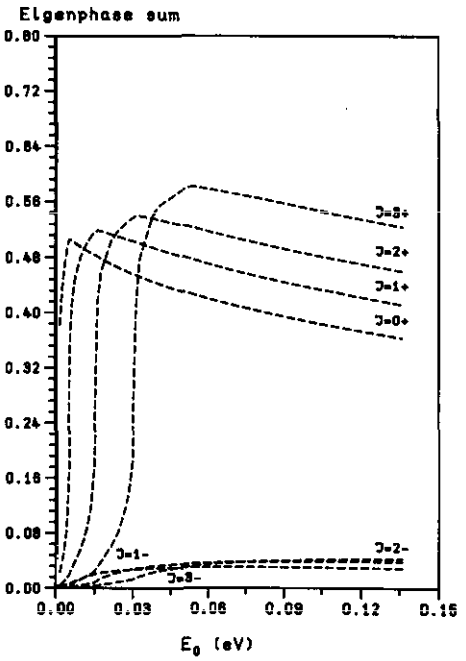

Figure 4. Eigenphase sums (rad) in the laboratory frame for different symmetries J and η.

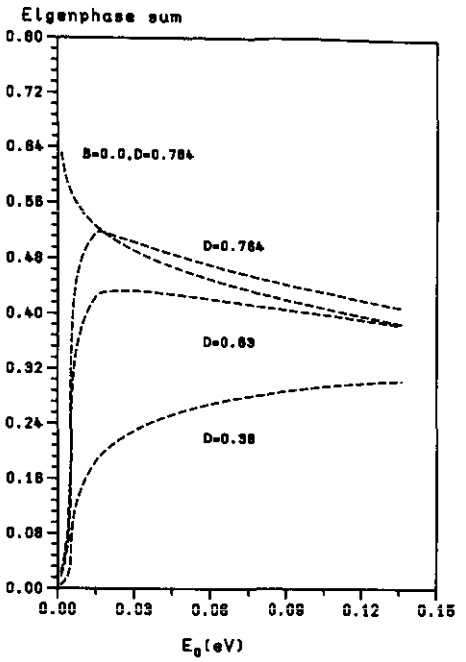

Figure 5. Eigenphase sums (rad) in the laboratory frame for the total angular momentum $J = 1$ and different choices of dipole moment D(au). The upper curve ($B = 0$) corresponds to the body frame eigenphase sum in the FN approximation.

'adiabatic' effective interaction between channels coupled by the dipole interaction, it follows (Clark 1979) that the asymptotic form of the interaction potential is

$$V_i^J(r) = Bj_i(j_i+1) + (l_i(l_i+1)/r^2) + \gamma_i(D^2/Br^4) + \mathrm{O}(r^{-6}) \tag{10}$$

where each l_i,j_i identify a rotational channel for given total angular momentum J. Note that the meaning of 'adiabatic' here is different from that usually found in literature on electron–molecule scattering. It implies the use of a rotationally and orbitally adiabatic basis set in the space-fixed frame, sometimes called the method of perturbed stationary states (Levine 1969b). Specifically it corresponds to disregarding certain velocity-dependent terms in the equation of motion. A detailed discussion of the methodology of the 'adiabatic' theory in electron scattering from diatomic molecules is given by Clark (1978). We will not discuss the validity of this 'adiabatic' approximation at this point. The validity of it in near-threshold electron scattering from polar molecules seems not to have been fully understood. A calculation within the framework of the 'adiabatic' method in the near-threshold energy region was done by Engelking and Herrick (1984), who state that the 'adiabatic model breaks down when quantitative use of it is attempted' (for an application at larger incident energies see Clary and Henshaw (1987) and Mullaney and Truhlar (1978)). However, we will accept that the dipole interaction in the asymptotic region gives rise to a strong polarization interaction $-\alpha_D/r^{-4}$ with $\alpha_D \sim \gamma(D^2/B)$, generally orders of

magnitudes larger than those arising from the distortion of the molecular charge distribution (table 1). Given equation (10), it follows for $E_{\text{inc}} \to 0$, in accordance with O'Malley *et al* (1961), that

$$K_{\text{ss}}^{J} = \tau k + \kappa k^2 + \cdots \tag{11}$$

with $\kappa \sim \alpha_{\text{D}}$. Here $k^2/2m = E_{\text{inc}}$ is the energy above the threshold $E_{j=J}$ and $-\tau$ is the scattering length. A logarithmic plot of the energy dependence of K_{ss}^{J} for $J = 0, 1, 2, 3$ is shown in figure 6. At low incident energies such as $k^2 = 1.0 \times 10^{-5}\ a_0^{-2}$ there are deviations from the standard Wigner scaling $\sim k^{2l+1}$ (Wigner 1948), which can be attributed to the large second term of equation (11) involving the dipole polarizability α_{D}. The values of τ and κ determined by a least-squares fit in the energy range from 1.0×10^{-5} up to $1.8 \times 10^{-4}\ a_0^{-2}$ are given in table 6. The absolute value for the scattering length is largest for $J = 0$ ($\tau = 67.6$ au), and decreases with increasing J. We find, by fitting to equation (11), a large negative value of $\kappa = -2037$ for $J = 0$ and values of decreasing magnitude for $J > 0$. The values of these parameters obtained by fitting our *ab-initio* results are sensitive to the choice of the radius r_{F} of the frame transformation, especially for larger values of J. Results of a more detailed study of this behaviour will be published elsewhere. Assuming a long-range component $\sim r^{-2}$ of the interaction potential, the low-energy expansion for K_{ps}^{J} corresponding to rotational excitation follows from the K-matrix Born approximation (Bardsley and Nesbet 1973),

$$K_{\text{ps}}^{J} = c_1(k^2 + \Delta)^{-1/4}k^{1/2} + c_2(k^2 + \Delta)^{-5/4}k^{5/2} + \cdots. \tag{12}$$

Here c_1, c_2 are constants and Δ is the difference in energy between the two thresholds $E_{j=J}$ and $E_{j=J-1}$. Equation (12) indicates a low-energy scaling law $\sim k^{1/2}$ appropriate to s-wave scattering in the new channel $j = J$ opening at threshold. Values of t ($= \lim_{k\to 0} K_{\text{ps}}^{J}(k)/k^{1/2}$) obtained from a least-squares fit in the energy region specified earlier are given in table 6. The absolute values of t increase slightly with increasing J. Generally for each value of J we have M open channels below and $N = M + n$ open channels above each rotational threshold $E_{j=J}$. For small k the full K-matrix above threshold is of the form (Nesbet 1980):

$$\begin{pmatrix} K_{MM} & K_{Mn} \\ K_{nM} & K_{nn} \end{pmatrix} = \begin{pmatrix} \tan\eta & tk^{1/2} \\ t^{\dagger}k^{1/2} & \tau k \end{pmatrix}. \tag{13}$$

This holds for s-wave scattering in the n channels opening at threshold. The K-matrix elements that correspond to background scattering have finite values at the rotational thresholds. These matrix elements are collected in the $M \times M$ matrix $\tan\eta$. If only s and p partial waves are included in the rotational basis set for each J, then $M = n = 1$, and

$$\begin{pmatrix} K_{MM} & K_{Mn} \\ K_{nM} & K_{nn} \end{pmatrix} = \begin{pmatrix} K_{\text{pp}}^{J} & K_{\text{ps}}^{J} \\ K_{\text{sp}}^{J} & K_{\text{ss}}^{J} \end{pmatrix}. \tag{14}$$

As described in detail by Bransden (1970) the $M \times M$ submatrix K above the threshold is related to the K'-matrix below the threshold by analytic continuation of the unitary S-matrix, including closed channels. The discontinuity at threshold of the energy derivatives of the K and K' elements leads to cross section Wigner

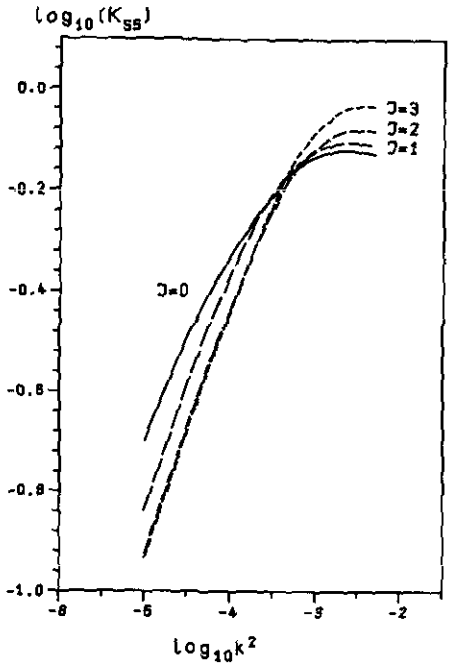

Figure 6. Logarithmic plot showing the energy dependence of K^J_{ss} $(k^2(a_0^{-2}))$.

Table 6. Parameters describing the low-energy behaviour of K^J_{pp}, K^J_{ps} and K^J_{ss} according equations (11) and (13). The β values refer to equation (15). See text for further explanation.

J	M	n	tan η	t	τ	κ	$\beta(a_0^{-1})$	$\beta^2/2$ (meV)
0	0	1	—	—	67.6	−2037.0	0.0147	3.0
1	1	1	0.294	−5.78	50.4	−786.9	0.0242	7.9
2	3	1	0.367	−5.71	38.9	−300.7	0.0348	16.4
3	6	1	0.421	−5.83	37.7	−200.7	0.0386	20.3

cusps and rounded steps. Knowing the leading terms of the K-matrix elements, the multichannel theory of threshold effects can be expressed in a form which separates background scattering from resonance effects or virtual state singularities (Nesbet 1980). The S-matrix $S(k)$ has a pole at $k = -i\beta$, corresponding to a virtual state if $\beta > 0$ or to a resonance or bound state below threshold if $\beta < 0$, where β is defined as

$$\beta = (\tau - t^{\dagger} \sin \eta \cos \eta t)^{-1}. \tag{15}$$

The calculated values of β (table 6) indicate that the multichannel threshold structures are due to virtual states. The characteristic threshold behaviour of the cross section in this case is that there is no structure immediately below the threshold, but an excitation peak rises to a maximum value near an energy of β^2, in Rydberg units, above the threshold (Nesbet 1980). We find β corresponding to energy 2.97 meV for $J = 0$, increasing with J. For $J = 0$ the present result is eight times larger than the

value 0.38 meV computed by Fabrikant (1983), who applied the frame-transformation effective range theory (FTERT). This earlier study depended on empirical values of the FN electron affinity of HF, which was not known to high accuracy.

3.2.4. Cross sections. In figure 7 the largest partial cross sections $\sigma_{j=j}^{J=2}$, are shown as an example. As follows from the threshold behaviour of the K-matrix elements (see figures 2(*a*)–(*c*)), the partial cross section $\sigma_{j=J-1\to J-1}^{J=2}$ corresponding to background scattering shows a cusp with infinite slope at threshold $E_{j=J}$. For cross sections $\sigma_{j=J\to J}^{J}$ corresponding to scattering in the new channels opening at $E_{j=J}$ it follows for small k from equation (11) (O'Malley 1963)

$$\sigma_{j=J\to J}^{J} = 4\pi[\tau^2 + 2\tau\kappa k + \cdots]. \tag{16}$$

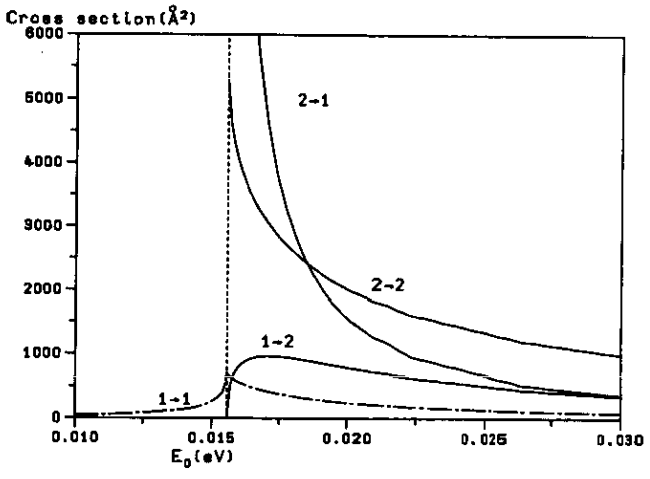

Figure 7. Energy dependence of the partial cross sections $\sigma_{j=j}^{J=2}$, near the threshold $E_{j=2}$ indicated by a vertical broken line.

Hence the elastic cross sections $\sigma_{j=J\to J}^{J}$ have large finite values as $k^2 \to 0$. The threshold excitation peak $\sigma_{1\to 2}^{J=2}$ rises as $\sim k$. The cross section for a de-excitation process is generally related to that of the inverse process (excitation) through the law of detailed balance. It follows (equation (7)) that the corresponding de-excitation cross section then necessarily diverges close to threshold as $\sim k^{-1}$. Hence, due to the de-excitation cross sections with $\Delta j = 1$ in electron scattering from polar molecules, we obtain an infinite cross section at each energy E_0 corresponding to a rotational threshold $E_j = Bj(j+1)$ $(j = 1, 2, 3, \ldots)$. If the cross sections are displayed as a function of incident energies, this is equivalent to zero incident energy since $E_{\text{inc}} = E_0 - Bj(j+1)$, where j describes the initial rotational state. Similarly to Coulombic scattering, there is no physical inconsistency in the fact that the pure dipole cross sections $\sigma_{j=J\to J-1}^{J}$ for $J > 0$ go to infinity, since the dipole field is screened by other charges at large distances in actual experimental situations (see, for example Taylor (1972)).

In figure 8 integrated cross sections computed according to equation (9) are shown for excitations from the lowest four initial states, summed over all possible

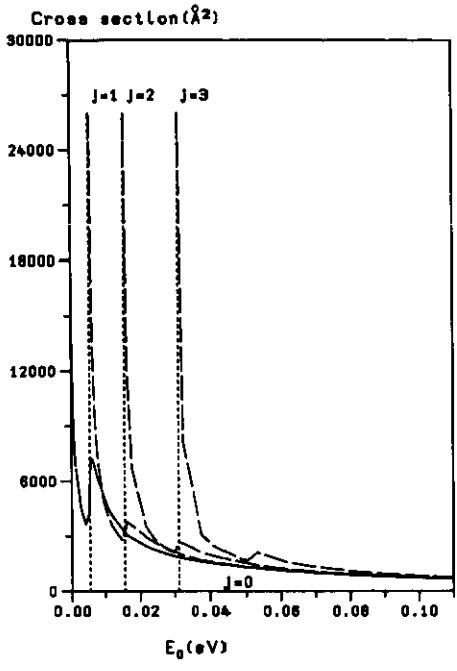

Figure 8. Energy dependence of the total integrated cross sections $\sigma_j = \sum_{j'} \sigma_{j \to j'}$ for initial states $j = 0, 1, 2$ and 3.

final states (i.e. open channels) $\sigma_j = \sum_{j'} \sigma_{j \to j'}$. As expected from the previous discussion, we obtain an infinite value at each threshold $E_{j=1,2,\ldots}$. The overall shape of each σ_j curve is determined by the partial cross sections $\sigma_{j \to j-1}^{J=j}$, $\sigma_{j \to j}^{J=j}$, $\sigma_{j \to j}^{J=j+1}$ and $\sigma_{j \to j+1}^{J=j+1}$, whereby the latter two are responsible for a cusp and an excitation peak at the threshold E_{j+1}.

As already stated in section 3, typical temperatures at which experiments have been performed are about 400 K. This means that the initial states must be weighted according to their relative statistical population. It follows for HF that the maximum is found for the state with $j = 2$ (23.4%) while for states with $j > 7$ the population is below 1%. The typical pattern one would obtain under these conditions (initial states weighted and summed over final rotational states) for the integrated cross section is shown in figure 9, in which the cross sections are displayed as a function of incident energy for the respective initial rotational states. Note that the curves for temperatures of 100 and 400 K approach the curve for 0 K with increasing incident energy. This is expected for the energy range in which the rotational level spacing loses importance and in which the adiabatic nuclei rotation approximation (ANR) for the scattering amplitude becomes valid (for a discussion see Shimamura (1984)). Note that detailed structures due to the rotation grow sharper at smaller temperatures. The threshold structures at $E_{\text{inc}} = B(j+1)(j+2) - Bj(j+1)$ are due to the contributions $\sigma_{j \to j}^{J=j+1}$ and $\sigma_{j \to j+1}^{J=j+1}$.

The angular dependence of total cross sections for the excitation of the $j = 2$ rotational state at different incident energies is shown in figure 10. The rotational channel $j = 3$ opens at $E_{\text{inc}} = 15.5$ meV and $j = 4$ at $E_{\text{inc}} = 36.3$ meV. One first notices the strong forward peaking which is enhanced at increasing energies. As can

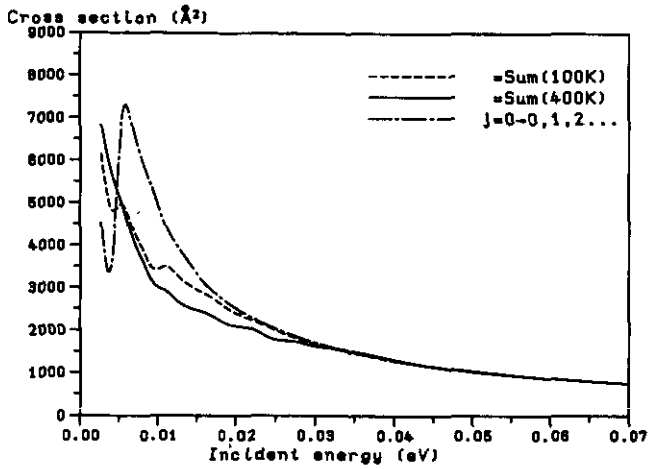

Figure 9. Rotationally summed integrated cross sections as a function of incident electron energy. The initial states are weighted according to their relative statistical population for temperatures of 400, 100 and 0 K.

be judged from figure 11, in which the individual contributions at 31 and 68 meV are displayed, the forward peaking is mainly due to transitions with $\Delta j = 1$. The differential cross section for the rotational elastic process $j = 2 \rightarrow 2$ (predominantly s-wave scattering) is much more isotropic.

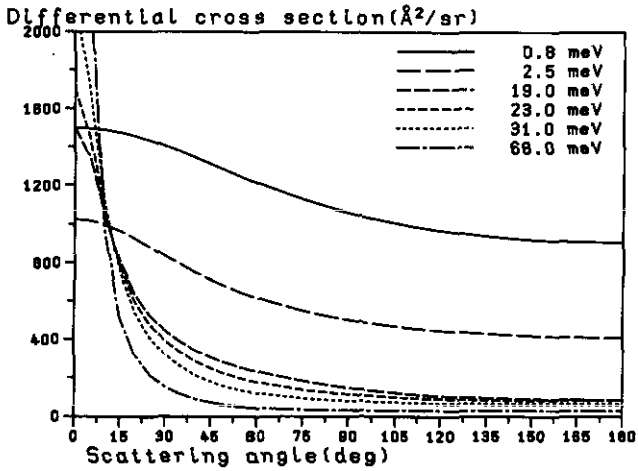

Figure 10. Total differential cross sections for the excitation from the rotational state $j = 2$ at different incident energies close to threshold.

An analysis of the A_L coefficients of equation (9) indicates that the forward peaking of rotational transitions with $\Delta j = \pm 1$ is affected by the J convergence of the corresponding transition matrix elements. If there is only one dominant contributor, as found for very low impact energies, the differential cross sections are more isotropic. Consistent with the Born dipole approximation, the forward peaking is more pronounced for larger incident energies.

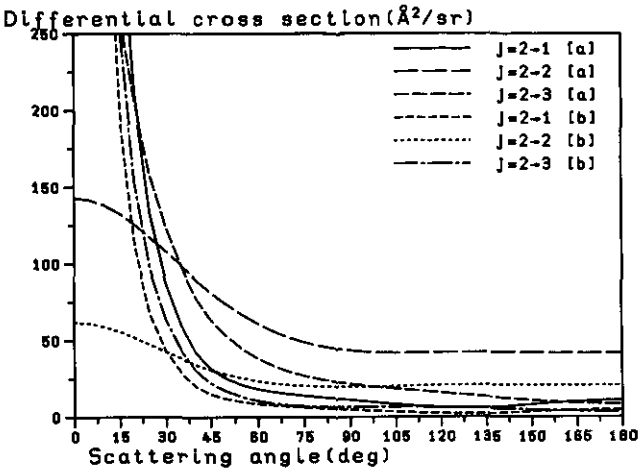

Figure 11. Differential cross sections for individual contributions $j = 2 \rightarrow j'$ at small incident energies of 31 meV [a] and 68 meV [b].

3.3. Results at higher energies

In this section we present the results of calculations in the energy range 0.6–6 eV. Calculations at various levels of accuracy are compared with each other and with the results of measurements published by Rädle *et al* (1989). In order to separate short-range effects from those of the long-range dipole potential, we have solved the laboratory-frame close-coupling equations including only the static dipole potential. In these dipole close-coupling (DCC) calculations we have chosen a potential cutoff at $r_0 = 2.3\ a_0$, which was also used in calculations within the framework of the FBA. DCC will account for all higher-order effects of the dipole potential. In analogy to the exact treatment based on the variational R-matrix method (VAR) we have used formula (9) for approximating the transition matrix elements for $J > 6$ (see section 2.3.2). Rotationally summed differential cross sections at different incident energies are summarized in table 7. Figures 12 and 13 compare our results with the data of Rädle *et al* (1989) at 0.63 and 3.0 eV, respectively. Especially at large energies the agreement between the experimental (EXP) measurements and the full calculations (VAR) is good. The published experimental differential cross section was estimated to have an error of less than 20%. For the rotational partial cross sections shown in figures 12 and 13, the relative error due to the uncertainty of the rotational deconvolution procedure used and errors due to statistics and angular corrections are less than 10% in the angular range above 20° and 15% below 20°. (Rädle *et al* 1988).

At 0.63 eV the scattering is mainly determined by the dipole interaction and its higher-order effects which affect the rotational transition $\Delta j = 0, 2$. For both transitions there is a significant rise in the forward direction, as indicated in table 8 and in figure 12. Here DCC is responsible for about 60% of the $j = 0 \rightarrow 0$ and about 80% of the $0 \rightarrow 2$ transition. Rädle *et al* (1988) discussed the second Born dipole approximation (SBA) (Feinberg *et al* 1986). These values are also included in table 8. Contrary to the DCC result which treats the dipole term essentially exactly, the SBA seems only to provide for about 20% of the $J = 0 \rightarrow 0$ cross section. Contrary to the measurements, the theoretical values for the $j = 0 \rightarrow 2$ transition are significantly

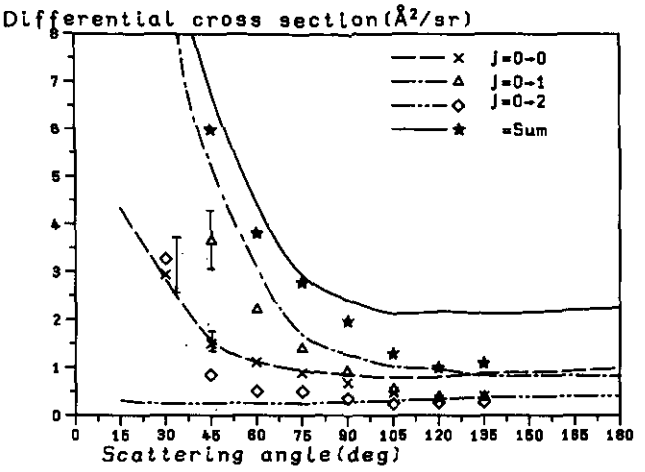

Figure 12. Rotationally partial differential cross sections at 0.63 eV. Summed cross section is indicated by 'sum'.

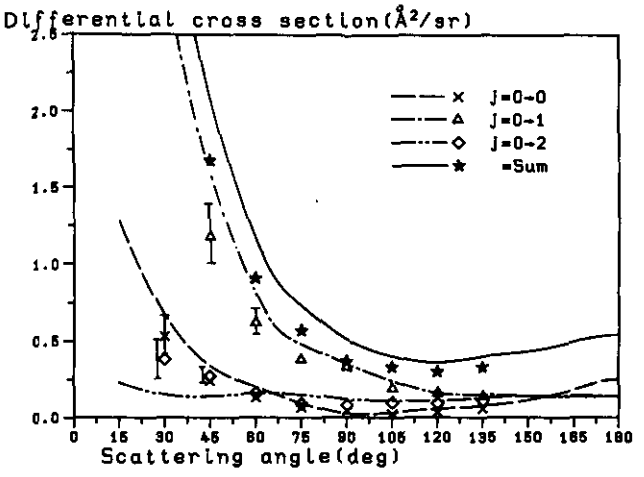

Figure 13. Rotationally partial differential cross sections at 3.0 eV. Summed cross section is indicated by 'sum'.

smaller in the forward direction. However, the general shape is well reproduced in all cases. For the calculated cross section $j = 0 \rightarrow 0$ we obtain a minimum around 110°. At larger energies short-range effects and polarizabilities gain importance (see section 2.3.3). At 3 eV (table 7 and figure 13) the DCC in comparison with the full calculations (VAR) accounts only for 30% of the $j = 0 \rightarrow 0$ transition and about 25% in the case of $j = 0 \rightarrow 2$. Similarly to the situation at 0.63 eV impact energy, both the $j = 0 \rightarrow 0$ and the $j = 0 \rightarrow 2$ cross section are forward peaked. For $j = 0 \rightarrow 2$ the forward peaking is not as marked as is found experimentally. For angles larger than 60° the FBA as well as the DCC results underestimate the $j = 0 \rightarrow 1$ cross section appreciably. The VAR results are in good agreement with the measurements. At 3 eV the present results can be compared with the results of the close-coupling calculations (CC) of Norcross (1987), summarized in table 8. For all the rotational

Table 7. Rotationally summed differential cross sections at different energies for excitations from $j = 0$: (*a*) present *ab-initio* results (VAR); (*b*) present dipole close coupling valculation (DCC); (*c*) result in FBA; (*d*) experimental results of Rädle *et al* (1988) (EXP).

Θ (deg)		15	30	45	60	75	90	105	120	135
$E = 0.63$ eV	*a*	64.46	16.14	7.01	4.56	2.94	2.42	2.14	2.18	2.14
	b	62.38	14.32	5.72	3.88	2.51	1.47	1.25	1.15	1.07
	c	60.06	15.03	6.70	3.79	2.46	1.74	1.32	1.07	0.91
	d	—	16.34	5.98	3.81	2.79	1.98	1.30	1.00	1.09
$E = 1.2$ eV	*a*	33.47	8.50	3.74	2.22	1.51	1.12	0.92	0.86	0.88
	b	32.33	7.33	2.88	1.76	1.10	0.63	0.52	0.47	0.43
	c	31.38	7.73	3.37	1.84	1.15	0.78	0.57	0.44	0.36
	d	—	7.99	3.49	2.13	1.53	1.03	0.75	0.63	0.66
$E = 1.5$ eV	*a*	26.78	6.89	3.05	1.76	1.18	0.87	0.72	0.67	0.70
	b	25.73	5.80	2.26	1.35	0.85	0.46	0.35	0.30	0.28
	c	25.04	6.12	2.63	1.42	0.87	0.58	0.41	0.31	0.25
	d	—	7.17	2.97	1.55	1.04	0.72	0.65	0.53	0.56
$E = 3.0$ eV	*a*	14.13	4.30	2.14	1.17	0.73	0.51	0.40	0.36	0.40
	b	13.60	2.75	1.02	0.55	0.31	0.15	0.092	0.083	0.066
	c	12.35	2.90	1.17	0.58	0.33	0.19	0.12	0.075	0.053
	d	—	3.81	1.68	0.91	0.57	0.37	0.33	0.30	0.33
$E = 6.0$ eV	*a*	7.44	2.54	1.36	0.75	0.48	0.38	0.29	0.24	0.29
	b	6.09	1.24	0.42	0.18	0.080	0.029	0.012	0.008	0.004
	c	6.01	1.30	0.46	0.18	0.077	0.032	0.013	0.005	0.002
	d	10.16	2.79	1.23	0.79	0.43	0.29	0.28	0.26	0.29

transitions $\Delta j = 0, 1$ and 2 there is a good agreement in shape and absolute values with the present (VAR) and the CC results. However the present values are slightly larger than those obtained from the CC calculations at all scattering angles. For the $j = 0 \rightarrow 0$ cross section in both theoretical investigations as well as in the experiment a minimum at an angle near 100° is found.

4. Summary and conclusions

We have presented an *ab-initio* method, based on the variational R-matrix method and the frame-transformation theory, which includes non-adiabatic rotational effects. For vibrationally elastic scattering these effects are expected to be important at incident electron energies of the order of the rotational constant B. This expectation is confirmed in the present work for the example of electron scattering by the polar molecule HF. The origin and character of the threshold structures are discussed quantitatively. In the body frame, the threshold law can be described by an analytic formula (equation (7) here) in terms of dipole functions. Similarly, in the laboratory frame, the long-range (rotating) dipole leads to a slow rate of convergence of the laboratory-frame scattering equations in total angular momentum J. Even with the present methods, exact solution of the laboratory-frame scattering equations is a time-consuming process, and it is useful to have some estimate of optimal values of the free parameters of the calculations. For this reason, we have carried out studies to

Table 8. Differential cross sections for rotational transitions $j = 0 \rightarrow 0, 1, 2$ at 0.63 and 3 eV: (*a*) present full calculation (VAR); (*b*) close coupling (CC) results of Norcross (1987); (*c*) present DCC calculation; (*d*) result in SBA; (*e*) present results in FBA; (*f*) experimental results of Rädle *et al* (1988).

Θ (deg)		15	30	45	60	75	90	105	120	135
$E = 0.63$ eV										
$0 \rightarrow 0$	*a*	4.34	2.84	1.58	1.12	0.94	0.85	0.79	0.81	0.89
	c	2.95	1.61	0.85	0.64	0.57	0.52	0.45	0.44	0.43
	d	1.70	0.55	0.12	0.01	—	—	—	—	—
	f	—	2.94	1.50	1.11	0.89	0.69	0.49	0.34	0.40
$0 \rightarrow 1$	*a*	59.31	13.07	5.18	3.19	1.70	1.28	1.03	0.97	0.84
	c	59.06	12.50	4.62	2.82	1.74	0.76	0.59	0.50	0.40
	e	60.06	15.03	6.70	3.74	1.90	1.75	1.33	1.07	0.91
	f	—	10.31	3.65	2.21	1.40	0.93	0.56	0.39	0.38
$0 \rightarrow 2$	*a*	0.31	0.24	0.25	0.25	0.25	0.28	0.31	0.35	0.39
	c	0.27	0.22	0.25	0.23	0.20	0.19	0.20	0.20	0.20
	f	—	3.27	0.84	0.50	0.50	0.36	0.25	0.27	0.28
$E = 3.0$ eV										
$0 \rightarrow 0$	*a*	1.28	0.67	0.34	0.20	0.093	0.025	0.031	0.058	0.077
	b	0.98	0.42	0.21	0.10	0.05	0.03	0.02	0.03	0.05
	c	0.35	0.14	0.049	0.029	0.025	0.020	0.016	0.015	0.013
	f	—	0.53	0.24	0.13	0.068	0.044	0.023	0.033	0.059
$0 \rightarrow 1$	*a*	12.61	3.47	1.66	0.81	0.48	0.35	0.24	0.16	0.15
	b	—	—	—	0.64	0.39	0.28	0.21	0.18	0.15
	c	12.20	2.57	0.93	0.49	0.36	0.11	0.054	0.049	0.035
	e	12.35	2.90	1.17	0.58	0.32	0.19	0.12	0.075	0.053
	f	—	2.90	1.18	0.62	0.38	0.33	0.19	0.16	0.14
$0 \rightarrow 2$	*a*	0.23	0.15	0.14	0.16	0.15	0.12	0.11	0.11	0.13
	b	0.15	0.12	0.09	0.08	0.08	0.08	0.09	0.10	0.10
	c	0.050	0.038	0.040	0.035	0.026	0.023	0.021	0.018	0.016
	f	—	0.38	0.27	0.16	0.091	0.081	0.099	0.093	0.11

determine the range of validity of each of the various approximations used here. An understanding of the range of validity of these gives useful insight into the physics of the scattering process. We have discussed the FBA as well as the UFBA, which accounts to some extent for second-order effects. The UFBA seems to be a good approximation in the low-energy range, which is predominantly determined by the dipole interaction. The present methodology makes it possible to extend exact CC calculations, carried out for J up to some value J_{max}, first by UFBA up to some value J_{UFBA}, then, using Born closure as in equation (9), to sum over all higher J values.

For energies near the rotational thresholds we find structures due to rotationally non-adiabatic effects. We have studied the threshold laws governing the low-energy behaviour of the calculated K-matrix elements. From a low-energy expansion we have shown that, in the case of vibrationally elastic scattering, the multichannel threshold structures are associated with virtual states. The threshold scaling laws for rotational elastic scattering show remarkable deviations from the Wigner law, due to the large r^{-4} effective dipole-polarization potential. The low-energy behaviour of the

K-matrix elements leads to the corresponding threshold laws for the cross sections. For the de-excitation cross sections $j \rightarrow j-1$, in the case of a polar molecule it follows from the threshold scaling of K-matrix elements that there is an infinite cross section as the incident energy of the electron goes to zero, similarly to the well known case of Coulomb scattering. In the energy range 0.6–6 eV good agreement was found between differential cross sections measured by Rädle *et al* (1980) and the theoretical cross sections computed here. Especially at larger energies, the calculated values lie well within the error bars specified in the measurements.

Non-adiabatic rotational effects have not been previously computed in the context of an *ab-initio* electronic FN calculation, starting from a variational R-matrix calculation. The detailed threshold analysis carried out here emphasizes the qualitative fact that for polar molecules FN models cannot, in principle, give correct results in the threshold region, because the analytic character of scattering matrices and cross sections as a function of energy is changed when molecular rotation is taken into account. This corresponds to the physical effect of screening or suppression of the long-range static dipole potential for a rotating molecule.

Vibrationally inelastic processes will be discussed in a subsequent paper. Analysis of such effects is needed for understanding the threshold peaks observed in vibrational excitation cross sections in molecules such as HF and HCl. Multichannel threshold analysis of the rovibronic scattering matrices, equivalent to that presented here will show whether the threshold structures are to be characterized as consequences of underlying virtual states or of true nuclear-excited resonances, and will follow this characterization if it changes with the vibrational quantum number.

Acknowledgments

The authors are grateful to P Botschwina for making available the values of the static polarizabilities as a function of internuclear distance. The computing time and services made available by the University of Bonn Computing Centre are gratefully acknowledged. We thank the Deutsche Forschungsgemeinschaft for financial support.

References

Arthurs A M and Dalgarno A 1960 *Proc. R. Soc.* A **256** 540
Baluja K L, Burke P G and Morgan L A 1982 *Comput. Phys. Commun.* **27** 299
Bardsley J N and Nesbet R K 1973 *Phys. Rev.* A **8** 203
Botschwina 1991 Private communication
Bransden B H 1970 *Atomic Collision Theory* (New York: Benjamin)
Buckley B D, Burke P G and Noble C J 1984 *Electron Molecule Collisions* ed I Shimamura and Takayanagi (New York: Plenum)
Burke P G and Noble C J 1986 *Comment. At. Mol. Phys.* **18** 181
Chandra N 1977 *Phys. Rev.* A **6** 84
Chang E S and Fano U 1972 *Phys. Rev.* A **6** 173
Clark C W 1979 *Phys. Rev.* A **20** 1875
—— 1984 *Phys. Rev.* A **30** 750
Clary D C and Henshaw J P 1987 *Int. J. Mass Spectrosc. Ion Proc.* **80** 31
Engelking P C and Herrick D R 1984 *Phys. Rev.* A **30** 750
Fabrikant I I 1983 *J. Phys. B: At. Mol. Phys.* **16** 1269
Feinberg G, Suchet J and Amado R 1986 *Phys. Rev. Lett.* **57** 416
Gillan C J, Nagy O, Burke P G, Morgan L A and Noble C J 1987 *J. Phys. B: At. Mol. Phys.* **20** 4585

Golden D E, Lane N F, Temkin A and Gerjury E 1971 *Rev. Mod. Phys.* **43** 642
Itikawa Y 1978 *Phys. Rep.* **46** 117
Knoth G, Rädle M, Gote M, Ehrhard H and Jung K 1989 *J. Phys. B: At. Mol. Opt. Phys.* **22** 299
Lane N F 1980 *Rev. Mod. Phys.* **52** 29
Levine R D 1969a *J. Phys. B: At. Mol. Phys.* **2** 839
—— 1969b *Quantum Mechanics of Molecular Rate Processes* (London: Oxford University Press) section 3.2
Light J C and Walker R B 1976 *J. Chem. Phys.* **64** 4272
McLean L A and Yoshimine M 1967 *J. Chem. Phys.* **47** 3256
Morgan L A 1984 *Comput. Phys. Commun.* **31** 419
Morgan L A and Burke P G 1988 *J. Phys. B: At. Mol. Opt. Phys.* **21** 2091
Morgan L A, Burke P G and Gillan C J 1990 *J. Phys. B: At. Mol. Opt. Phys.* **23** 99
Morrison M A 1988 *Adv. At. Mol. Phys.* **24** 51
Mullaney N A and Truhlar D G 1987 *Chem. Phys. Lett.* **58.4** 512
Nesbet R K 1975 *Phys. Rev.* A **12** 444
—— 1979 *Phys. Rev.* A **19** 551
—— 1980 *J. Phys. B: At. Mol. Phys.* **13** L193
—— 1984 *J. Phys. B: At. Mol. Phys.* **17** L897
—— 1992 to be published
Nesbet R K, Noble C J and Morgan L A 1986 *Phys. Rev.* A **34** 2798
Norcross D W 1987 *Proc. Fourth Int. Swarm Seminar and Electron–Molecule Collisions Symp. (Tahoe City, CA 1985)* ed L C Pitchford, B V McKoy, A Chutjian and S Trajmar (New York: Springer) p 217
Norcross D W and Collins L A 1982 *Adv. At. Mol. Phys.* **18** 341
Noble C J and Nesbet R K 1984 *Comput. Phys. Commun.* **33** 399
O'Malley T F 1963 *Phys. Rev.* A **130** 1020
—— 1965 *Phys. Rev.* A **137** 1668
O'Malley T F, Spruch I and Rosenberg L 1961 *J. Math. Phys.* **2** 491
Rädle M, Knoth G Jung K and Ehrhard H 1989 *J. Phys. B: At. Mol. Opt. Phys.* **22** 1455
Rohr K and Linder F 1976 *J. Phys. B: At. Mol. Phys.* **9** 2521
Schneider B I and Collins L A 1982 *J. Phys. B: At. Mol. Phys.* **15** L335
Schneider B I, Le Dourneuf M and Burke P G 1979 *J. Phys. B: At. Mol. Phys.* **12** L365
Seaton M J 1961 *Proc. Phys. Soc.* **77** 174
—— 1966 *Proc. Phys. Soc.* **89** 469
Shimamura I 1984 *Electron–Molecule Collisions* ed I Shimamura and Takayanagi (New York: Plenum)
Sileo R N and Cool T A 1976 *J. Chem. Phys.* **65** 117
Taylor J R 1972 *Scattering Theory* (New York: Wiley)
Vo Ky Lan, Le Dourneuf M and Launay J M 1983 *Electron–Atom Electron–Molecule Collisions* ed J Hinze (New York: Plenum) p 161
Werner H J and Rosmus P 1980 *J. Chem. Phys.* **73,5** 2319
Wigner E P 1948 *Phys. Rev.* **73** 1002